The Use of Dark Matter Modulation to Constrain WIMP Mass and Infer Substructure in its Distribution

David Ellis

University of Nottingham

Weakly Interacting Massive Particles (WIMPs) can be detected directly through their elastic scattering off of nuclei. However, such experiments are subject to significant levels of background noise due to local radiation sources. Due to the Earth's orbit around the Sun the rate at which dark matter is detected is expected to oscillate with a period of one year. The primary background sources however are not expected to exhibit any such modulation. In this paper, using estimates of the distribution of dark matter we investigate how this modulation can be used to constrain the value for the WIMP mass. It is found that the amplitude of this modulation varies with WIMP speed and hence recoil energy. As such there exists a critical energy at which the amplitude is zero. This energy is dependent on the detector particle used. This critical energy can be used to set limits on the WIMP mass. We also find that discrepancies between the total number of detected collision events to that which is predicted theoretically can be used to infer the presence of substructure within the dark matter halo.

Contents

I.   Introduction

The existence of dark matter has been inferred through various astronomical observations since the early 1900's. Astronomers such as Jan Oort and Fritz Zwicky used the idea of dark matter to explain the observed motion of stars and galaxies respectively [1, 2]. They noted that the combined masses of the visible objects within the respective systems was not sufficient to keep objects with such high velocities from escaping. Later, strong evidence for the existence of dark matter came from the rotation curves of spiral galaxies [3].

Unlike ordinary matter, dark matter is not thought to interact though electromagnetism. As a consequence the relative abundance of dark matter influences the anisotropies observed within the microwave background radiation. Microwave space telescopes such as the Planck telescope have been used to measure these anisotropies and thus, determine the energy density of the universe that must come from dark matter. It has hence been determined that dark matter outweighs ordinary, baryonic dark matter by a factor of about five to one [4].

Further evidence for the presence of dark matter comes from gravitational lensing. Due to general relativity, gravity from massive objects such as galaxies has the ability to bend the path of light. As such the images of background objects can be distorted in a process known as gravitational lensing. This distortion can be used not only to determine the mass within a region of space but also to determine its distribution and therefor map the distribution of dark matter [5].

Since dark matter only weakly interacts with ordinary matter, we do not currently know what dark matter is composed of. The most prominent candidate to date, and the focus of this paper, is the weakly interacting massive particle (WIMP). These particles are expected to have masses in the range of around 10 to 1000 times the mass of a proton. As suggested by their name they only interact weakly with ordinary matter as well as being electrically neutral [6]. They are also predicted to be their own anti-particle, annihilating each other since the early universe leading to the density observed today.

There are a number of ways in which WIMPs can be studied. These include producing them in particle colliders such as the Large Hadron Collider [7] and through observing the products of their annihilation in the form of high energy gamma rays or anti-matter [8]. The focus of this paper however, is the method of direct detection through the elastic scattering of WIMPs off nuclei. When WIMPs collide with nuclei they transfer some of their kinetic energy. This energy is then detected in the form of heat, ionization and light [9]. However, radiation emitted from the Sun and sources local to the detector impose a large amount of background noise on these experiments. Some of this background is avoided by building detectors underground. Many collaborations are trying to detect these particles using detectors composed of materials such as xenon [10], germanium [11] and multi-element crystals such as sodium iodide [12].

As the Earth travels through the galaxy it also moves through the galactic dark matter halo. This dark matter almost entirely passes through the Earth without interacting with any of the Earths matter. However, there is a small chance for an interaction to occur and hence a chance for the dark matter to be detected. Due to the orbit of the Earth around the Sun the rate at which these particles are detected is expected to modulate throughout the year.

In June the Earth's velocity is roughly parallel to that of the Sun, such that the speed at which we travel through the dark matter halo is at a maximum. We would therefore expect the rate of detection to be highest at this time. Conversely, the direction of Earth's travel in December is roughly anti-parallel to that of the Sun, at this point detection is expected to be at its lowest [13]. This type of modulation is not expected to be seen for most of the primary background sources. Therefore, detecting this modulation is a 'smoking gun' for the presence of dark matter.

The specific behaviour of the modulation with respect to the recoil energy of collisions is dependent on the distribution of the WIMPs, as well as their physical properties. In this paper we investigate how the modulation of dark matter can therefore be used to constrain the WIMP mass and infer properties about the distribution of dark matter within the galaxy.

II.   Theory

A.   Detection

In a direct detection experiment a WIMP of mass M_χ collides with a detector nucleus of mass M, transferring momentum q. The target nucleus recoils with kinetic energy E_{nr}. Assuming the collision is perfectly elastic, this relates to a minimum WIMP speed relative to the nucleus given by

$$v_{\min} = \sqrt{\frac{ME_{nr}}{2\mu^2}}, \tag{1}$$

where $\mu \equiv M_\chi M/(M_\chi + M)$ is the reduced mass of the WIMP-nucleus system. Then assuming that the collisions are elastic the differential rate of collision events per unit of detector mass is given by

$$\frac{dR}{dE_{nr}} = \frac{1}{2M_\chi\mu^2}\sigma(q)\rho_\chi\eta(v_{\min}(E_{nr}),t), \tag{2}$$

where $\sigma(q)$ is the effective scattering cross-section, ρ_χ is the local dark matter density and $\eta(v_{\min}(E_{nr}),t)$ is the mean inverse speed [13]. This is given by the inverse velocity integral over the dark matter distribution $f(v,t)$

$$\eta(v_{\min}(E_{nr}),t) = \int_{v>v_{\min}} d^3v\,\frac{f(v,t)}{v}. \tag{3}$$

This mean inverse speed changes over a period of one year and is the term in equation 2 which drives the modulation in detection rate.

The variation of the differential detection rate over a year is shown primarily by the amplitude of the modulation. Since it is known that the detection rate peaks and troughs in June and December respectively, the amplitude is given by the equation

$$A_{dR/dE} \approx \frac{1}{2}\left[\frac{dR}{dE_{nr}}(\text{June 1}) - \frac{dR}{dE_{nr}}(\text{Dec 1})\right]. \tag{4}$$

B.   Distribution

1.   Simplified SHM

The dark matter halo through which the Earth passes is likely to be smooth in nature. Through dynamical observations of the Milky Way the local dark matter density has been found to be roughly $0.4\,\text{GeV cm}^{-3}$ [14]. The standard halo model (SHM) is often taken to be the simplest; a viralised isothermal sphere with an isotropic Maxwellian velocity distribution. This distribution is given by

$$f(v) = \left(\frac{1}{\pi v_0^2}\right)^{3/2} e^{-v^2/v_0^2}, \tag{5}$$

where v_0 is the most probable speed with a value approximately equal to the speed of the Sun through the galaxy. This speed is related to the velocity dispersion σ_v through the equation

$$v_0 = \sqrt{2/3}\,\sigma_v. \tag{6}$$

Since the Earth orbits the Sun the observed distribution changes throughout the year. We can account for this by rewriting the distribution as

$$f(v,t) = \tilde{f}(v_{\text{obs}}(t) + v). \tag{7}$$

Here the velocity $v_{\text{obs}}(t)$ is the velocity of the detector relative to the dark matter rest frame. Hence, it is a combination of the motion of the Sun relative to the dark matter rest frame v_{Sun} and the velocity of the Earth relative to the Sun $v_{\text{Earth}}(t)$

$$v_{\text{obs}}(t) = v_{\text{Sun}} + v_{\text{Earth}}(t) \,. \tag{8}$$

If the dark matter is smooth and non-rotating then v_{Sun} is simply a combination of the velocity of the local stellar neighbourhood in galactic coordinates $v_{\text{loc}} = (0, v_{\text{rot}}, 0)$ and the Sun's peculiar velocity $v_{\text{pec}} = (11.1, 12.2, 7.3)$ [15]. The Sun's orbital speed through the galaxy is observed to be $v_{\text{rot}} = 218 \text{ km s}^{-1}$ [16].

Then, assuming a perfectly circular orbit, the velocity of the Earth relative to the Sun is given by

$$v_{\text{Earth}}(t) = v_{\text{Earth}}[\hat{\varepsilon}_1 \cos\omega(t - t_1) + \hat{\varepsilon}_2 \sin\omega(t - t_1)]\,, \tag{9}$$

where $\omega = 2\pi/\text{yr}$ and the speed of Earth's rotation $v_{\text{Earth}} = 29.8 \text{ km s}^{-1}$. The unit vectors $\hat{\varepsilon}_1$ and $\hat{\varepsilon}_2$ give the directions of the Earth's motion at the spring equinox and summer solstice respectively. In galactic coordinates $\hat{\varepsilon}_1 = (0.9931, 0.1170, -0.01032)$ and $\hat{\varepsilon}_2 = (-0.0670, .04927, -0.8676)$ [17].

Since $v_{\text{Sun}} \gg v_{\text{Earth}}$ the equation for the magnitude of $v_{\text{obs}}(t)$ can be simplified by making the approximation

$$v_{\text{obs}}(t) \approx v_{\text{Sun}} + b v_{\text{Earth}} \cos\omega(t - t_0)\,, \tag{10}$$

where t_0 is the time at which the $v_{\text{obs}} \approx v_{\text{Sun}} + b v_{\text{Earth}}$ and $b \equiv \sqrt{b_1^2 + b_2^2}$ is a geometrical factor for $b_i \equiv \hat{\varepsilon}_i \cdot \hat{v}_{\text{Sun}}$. Performing the calculations we find that $b = 0.4896$.

Applying this to the modified dark matter distribution given by equation 5, the time varying nature of the distribution is realised as demonstrated in figure 1. As such the mean inverse speed, the quantity relating to the detection rate, also changes with time.

Figure 1 - Velocity distribution modulation predicted for June 1st and December 1st using the standard halo model.

For this, simple Maxwellian distribution, the mean inverse speed has a simple analytical equation given by

$$\eta(v_{\text{min}}, t) = \frac{1}{2 v_{\text{obs}}}[\text{erf}(x + y) - \text{erf}(x - y)]\,, \tag{11}$$

where $x \equiv v_{\text{min}}/v_0$ and $y \equiv v_{\text{obs}}/v_0$ [17]. This equation describes how the detection rate varies in time and, in part, how it depends on the recoil energy of the collision. As the mean inverse speed always peaks in June and December we can define the amplitude of the modulation of the mean inverse speed to be

$$A_\eta = \frac{1}{2}[\eta(v_{\text{min}}, \text{June 1}) - \eta(v_{\text{min}}, \text{Dec 1})]\,. \tag{12}$$

2.   Improved SHM

The simplified model as discussed so far neglects the fact that dark matter with a speed above some escape velocity v_{esc} will leave the galactic system and therefore not be detected. Through the study of the motion of high velocity stars, the escape velocity is found to be about 544 km s^{-1} [18]. This can be factored into the model simply by imposing that $\tilde{f}(v > v_{\text{esc}}) = 0$. This however, produces a sharp discontinuity in the distribution at the escape velocity which is not characteristic of what we would expect to see. This transition in the distribution near the
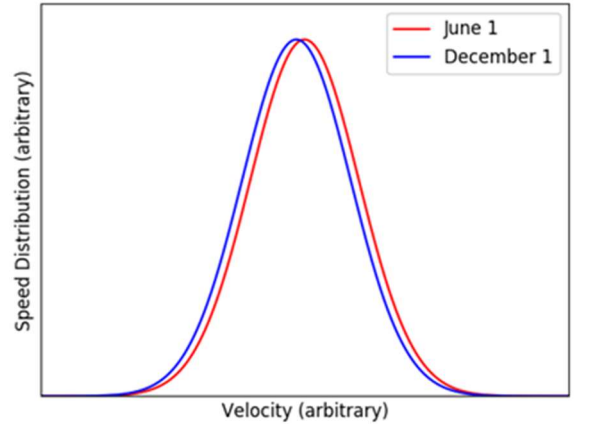
escape velocity can be improved by including an additional exponential term. The new distribution for the case in which $|v| < v_{\text{esc}}$ is given by

$$f(v) = \left(\frac{1}{\pi v_0^2}\right)^{3/2} [\exp(-v^2/v_0^2) - \exp(-v_{\text{esc}}^2/v_0^2)] \,. \tag{13}$$

The mean inverse speed for this distribution also has an analytical form given by

$$\eta(v_{\text{min}}) = \begin{cases} \frac{1}{v_{\text{obs}}}, & \text{for } z < y, x < |y - z| \\ \frac{1}{2N_{\text{esc}}v_{\text{obs}}}\left[\text{erf}(x + y) - \text{erf}(x - y) - \frac{4}{\sqrt{\pi}}\left(1 - x^2 - \frac{1}{3}y^2 - z^2\right)ye^{-z^2}\right], & \text{for } z > y, x < |y - z| \\ \frac{1}{2N_{\text{esc}}v_{\text{obs}}}\left[\text{erf}(z) - \text{erf}(x - y) - \frac{2}{\sqrt{\pi}}\left(y + z - x - \frac{1}{3}(y - 2z - x)(y + z - x)^2\right)e^{-z^2}\right], & \text{for } |y - z| < x < y + z \\ 0. & \text{for } v + z < x \end{cases} \tag{14}$$

where x and y are defined as before with $z \equiv v_{esc}/v_0$ and where

$$N_{\text{esc}} = \text{erf}(z) - \frac{2}{\sqrt{\pi}}z\left(1 + \frac{2}{3}z^2\right)e^{-z^2} \,, \tag{15}$$

is a normalization factor [17]. As we will see later, these corrections make little contribution to modulation of the detection rate.

3.   Dark Matter Stream

For a complete investigation into the modulation of dark matter the possible contribution of substructure within the dark matter halo must also be considered. Substructures such as debris flows and streams are unviralised and have the potential to significantly impact the observed modulation in dark matter detection. It is known that our galaxy is currently pulling a stream of material off of a smaller galaxy, Sagittarius. This is known as the Sagittarius stream [17]. It is logical to assume the matter within this stream includes dark matter. Astronomical investigations have found that this stream passes within a few kpc of our local stellar group [19]. This paper will therefore consider the possible effect of tidal streams.

Since the particles of which the stream is composed have not had sufficient time to interact with each other the velocity dispersion is small to negligible. If the stream is completely coherent ($\sigma_v = 0$) the velocity distribution is given by

$$\tilde{f}_{\text{str}}(v) = \delta^3(v) \,, \tag{16}$$

where $\delta^3(v)$ is the three dimensional Dirac delta function [17]. Naturally, this is not a very physical approximation as any stream will most likely have some level of velocity dispersion, but it serves as a good approximation for investigating the broader impacts of the stream.

The mean inverse speed of this simplified stream distribution is given by a Heaviside function

$$\eta(v_{\text{min}}) = \frac{1}{v'_{\text{obs}}}\theta(v'_{\text{obs}} - v_{\text{min}}) \,. \tag{17}$$

Here, the modified observed velocity is given by $v'_{\text{obs}} = v_{\text{obs}} - v_{\text{str}}$ where v_{str} is the speed of the stream relative to the detector [17]. In the simplified case in which $v_{\text{str}} = 0$ the observed velocity is equal to that given by equation 10, that is, $v'_{\text{obs}} = v_{\text{obs}}$.

The total differential detection rate is simply given by the sum of the detection rates calculated for the SHM and the stream using equation 2

$$\left(\frac{dR}{dE_{\text{nr}}}\right)_{\text{Total}} = \left(\frac{dR}{dE_{\text{nr}}}\right)_{\text{SHM}} + \left(\frac{dR}{dE_{\text{nr}}}\right)_{\text{Stream}} \tag{18}$$

C.   Cross Section

For direct detection experiments the rate of detection is proportional to momentum dependent WIMP-nucleus scattering cross section. When the WIMP momentum is small it scatters off the entire nucleus. However, as the momentum increases the de Broglie wavelength of the WIMP reduces in size causing the effective cross section to decrease [17]. This is encoded into the cross section by the form factor $F^2(q)$ through the equation

$$\sigma(q) = \sigma_0 F^2(q) \, , \tag{19}$$

where σ_0 is the scattering cross section in the limit in which momentum transfer is zero. When the momentum transfer, $q = 0$ the form factor $F^2(q) = 1$ [13]. For higher momentum transfers however $F^2(q) \ll 1$.

The total cross section is the sum of spin independent and spin dependent cross section

$$\sigma_0 = \sigma_{\text{SI}} + \sigma_{\text{SD}} \, . \tag{20}$$

The first order spin independent term is given by

$$\sigma_{\text{SI}} = \frac{4}{\pi} \mu^2 \big[Z f_{\text{p}} + (A - Z) f_{\text{n}} \big]^2 \, , \tag{21}$$

where the effective coupling of the WIMP to the proton and neutron is parameterized by f_p and f_{n} respectively, with the number of protons and neutrons respectively given by Z and $(A - Z)$ [20]. For most WIMP candidates the effective nucleon couplings are expected to be roughly equal ($f_p \approx f_n$). This allows the spin independent cross section to be approximated to

$$\sigma_{\text{SI}} = \frac{\mu^2}{\mu_{\text{p}}^2} A^2 \sigma_{\text{p,SI}} \, , \tag{22}$$

where μ_{p} is the reduced mass of the WIMP-proton system and $\sigma_{\text{p,SI}}$ is the spin independent cross section for WIMP-proton scattering [20].

For heavy detector nuclei $\mu^2 / \mu_{\text{p}}^2 \approx A^2$. Therefore, the spin independent cross section effectively scales as A^4. The same is not true for spin dependent interactions. This is one of the reasons why the spin independent term often dominates over the spin dependent term [17]. As such, to help simplify the model the WIMP-nucleus cross section is assumed to be purely spin independent. This assumption is particularly valid for heavy nuclei such as xenon which is the primary focus of this paper.

The WIMP-nucleon scattering cross section is significantly smaller than the geometrical cross section. Consequently, the specific value of this cross section has yet to be found. Instead, experiments such as those conducted by the XENON100 group provide an extensive 'exclusion zone' shown in figure 2, in which the WIMP-nucleon cross section cannot exist. To proceed with the investigation we must choose a value for this cross section. The specific value is not of great importance as it only acts to linearly scale the detection rate and plays no roll in its overall modulation. Therefore, based on the 2012 XENON100 results of figure 2 a value of $\sigma_{\text{p,SI}} = 2 \times 10^{-45}$ cm^2 will be used [21].

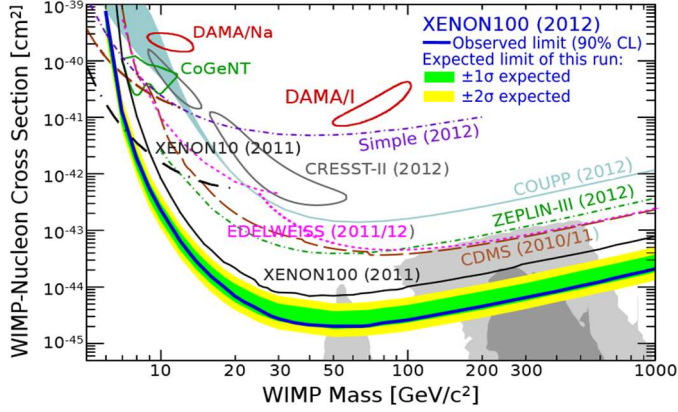Figure 2 – Spin-independent WIMP-nucleon scattering results from XENON100. The green and yellow bands show the expected 1σ and 2σ sensitivities of the experiment respectively. The consequential exclusion limit is shown in blue. For comparison, other experimental limits and detection claims are also presented. Figure modified from E. Aprile *et al.* 2013.

There are a number of approximations for the atomic form factor. For spin independent interactions one of the equations most commonly used in the Helm form factor given by

$$F(q) = 3e^{-q^2 s^2/2} \frac{\sin(qr_n) - qr_n\cos(qr_n)}{(qr_n)^3} , \qquad (23)$$

where constants a and s are approximately equal to 0.52 fm and 0.9 fm respectively with $c \approx 1.23A^{\frac{1}{3}} - 0.60$ fm and effective nuclear radius given by

$$r_n^2 = c^2 + \frac{7}{3}\pi^2 a^2 - 5s^2 . \qquad (24)$$

The Helm form factor was introduced to account for the soft edge of the nucleus by multiplying the form factor for a uniform sphere by a Gaussian [22]. While it is sufficient for this investigation, it is important to note that this equation is an approximation of the true form factor and neglects the effect of nuclear structure. The consequences of this structure are explored for WIMP scattering off xenon by L. Vietze *et al.* 2015 [23].

III. Results

A. Simplified SHM

1. Mean Inverse Speed

The mean inverse speed controls the frequency at which the detection rate is modulated. It is therefore important to understand its dynamics. The time varying mean inverse speed was investigated by plotting $\eta(v_{\min})$ as given by equation 11, using the detector speed given by equation 10. This was done for 3 different minimum detectable speeds; 0 km s^{-1}, 200 km s^{-1}, and 400 km s^{-1}. This is shown in figure 3 below.
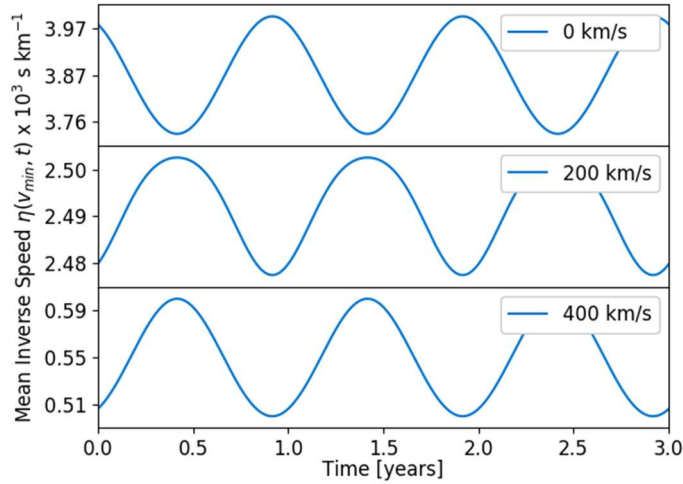
Figure 3 - Mean inverse speed $\eta(v_{\min})$ as a function of time for 3 different minimum detectable speeds; $0\,\mathrm{km\,s^{-1}}$, $200\,\mathrm{km\,s^{-1}}$, and $400\,\mathrm{km\,s^{-1}}$ calculated by modelling velocity distribution of dark matter as a simple Maxwellian distribution.

From figure 3 it can be seen that the sign of the amplitude changes between a $v_{\min} = 0\,\mathrm{km\,s^{-1}}$ and $v_{\min} = 200\,\mathrm{km\,s^{-1}}$. From this we can infer that there exists some WIMP speed between these two speeds at which the amplitude is zero. This speed relates to a recoil energy through equation 1.

As the mean inverse speed is also dependent on the minimum detectable WIMP speed. It is therefore also important to understand the characteristics of this relationship for some point in time. This was investigated further using equation 11 for the mean inverse speed and equation 10 for the detector speed but this time varying the minimum detectable speed $v_{\min}$. The result is shown in figure 4 below.
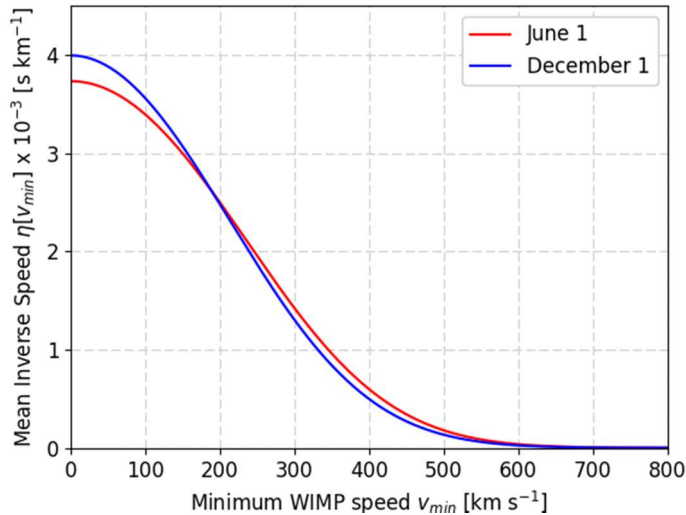

Figure 4 – Mean inverse speed $\eta(v_{\min})$ as a function of minimum detectable WIMP velocity $v_{\min}$ for the first of June and December, calculated be modelling velocity distribution of dark matter as a simple Maxwellian distribution.

The point at which the amplitude of modulation changes sign can clearly be seen on figure 4 as the point at which the mean inverse speed on the first of June and December is equal. This graph does not however illustrate the dependence on WIMP mass. This dependence arises from the relationship between the minimum detectable WIMP speed $v_{\min}$ and the nuclear recoil energy E_{nr} as given by equation 1. This is because in direct detection experiments the recoil energy is

measured through the resultant rise in detector temperature rather than directly measuring the WIMP speed.

The dependence on recoil energy can be illustrated by calculating the amplitude of the modulation of mean inverse speed A_η given by equation 10 as a function of the nuclear recoil energy E_{nr} for different WIMP masses M_χ. This was calculated for the case of a xenon based detector with an atomic mass of 131.3u as shown in figure 5 below
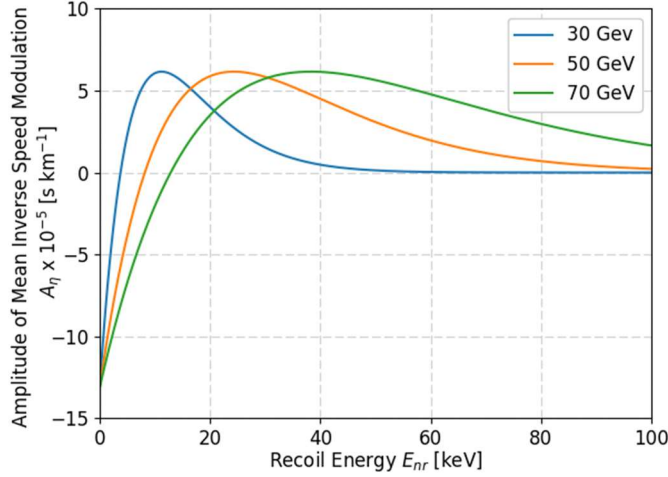

Figure 5 – Amplitude of Mean Inverse Speed Modulation A_η as a function of recoil energy E_{nr} for a xenon based detector predicted for WIMP masses 30, 50 and 70 GeV calculated by modelling velocity distribution of dark matter as a simple Maxwellian distribution.

From figure 5 it can be seen that the recoil energy for which the amplitude is zero, which we will call the critical energy, varies with the WIMP mass. For the cases displayed in figure 5 we see that a larger WIMP mass relates to a greater critical energy. This is central to being able to constrain the WIMP mass through direct detection experiments.

2.   Differential Detection Rate

Once the mean inverse speed is calculated, the differential detection rate can be found using equation 2. This is shown for the example of a WIMP with a mass of 70 GeV detected by a xenon based detector in figure 6 below. For the purpose of comparison, we focused on this example throughout the investigation.
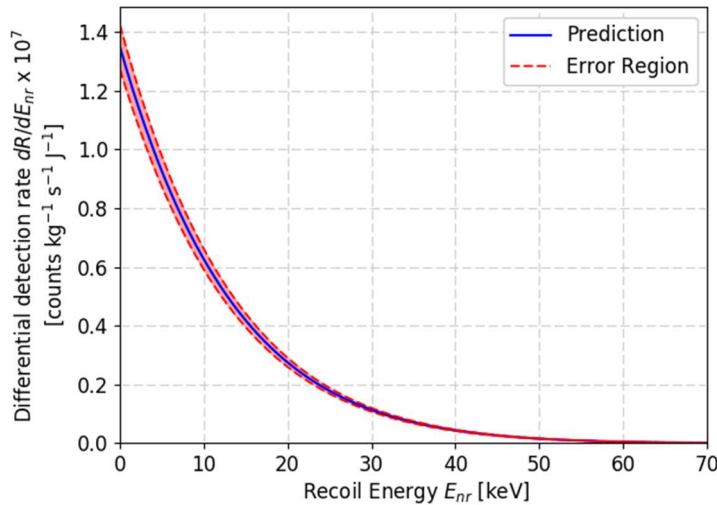

Figure 6 – Differential detection rate dR/dE_{nr} as a function of nuclear recoil energy E_{nr} for a WIMP mass of 70 GeV detected by a xenon based detector in June calculated by modelling velocity distribution of dark matter as a simple Maxwellian distribution.

Figure 6 shows that higher recoil energies are detected at a significantly lower rate than smaller recoil energies. The relationship is roughly that of an inverse exponential. The primary source of error in these values, neglecting those due to the cross section estimate, is the uncertainty in the local dark matter density ρ_χ. This however, we will see, does not factor into the predicted constraints on the WIMP mass.

Using this graph we can estimate of the total number of detection events we would expect to see in a given time period assuming the WIMP mass is $70\,\mathrm{GeV}$. This is done by integrating the curve with respect to recoil energy. Performing this integral numerically the number of counts is found to be $2.68 \times 10^{-8}\mathrm{s}^{-1}\mathrm{kg}^{-1}$.

This value can then be compared to experimental results by multiplying it by the exposure of the experiment. During the 2013 LUX experiments $370\,\mathrm{kg}$ of liquid xenon is used as a detector with an exposure of $1.4\,\times 10^4\,\mathrm{kg\,days}$. Given this exposure, using the detection rate predicted in figure 6 and assuming a WIMP mass of $70\,\mathrm{GeV}$, we would predict a total of $33 \pm 2\,\mathrm{counts}$ over the course of the experiment. This is consistent with the number the LUX group observed [24].

Once the direct detection rate is calculated the amplitude of detection rate modulation can be calculated using equation 4. This was calculated for 3 different WIMP masses as shown in figure 7.
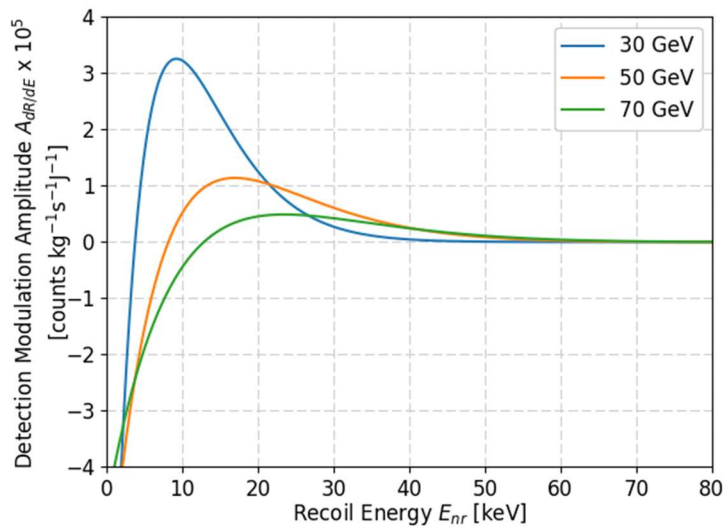

Figure 7 – Amplitude of detection rate modulation $A_{\mathrm{d}R/\mathrm{d}E}$ as a function of recoil energy E_{nr} for a xenon based detector predicted for WIMP masses 30, 50 and $70\,\mathrm{GeV}$ calculated by modelling velocity distribution of dark matter as a simple Maxwellian distribution.

Figure 7 shares similar characteristics to figure 5, this is expected due to the dependence of the detection rates on the mean inverse speed. Most importantly, the roots of the curves of corresponding WIMP masses are the same for both figures. This illustrates that the critical energy for some WIMP mass is determined entirely by the mean inverse speed function. We also see that the curve peaks in amplitude for higher WIMP masses are supressed compared to those of figure 5, and the curves also much less broad. This is due to the atomic form factor, given by equation 23, which is smaller for both larger WIMP masses and higher recoil energies.

3.   Critical Energy

Once the differential detection rate as a function of WIMP mass and recoil energy is known, it is possible to then numerically calculate the critical energy E_c as a function of WIMP mass. This was calculated using a basic root searching algorithm, the result of which is shown in figure 8 for the case of a xenon detector with a focus on the low mass range shown in figure 9.
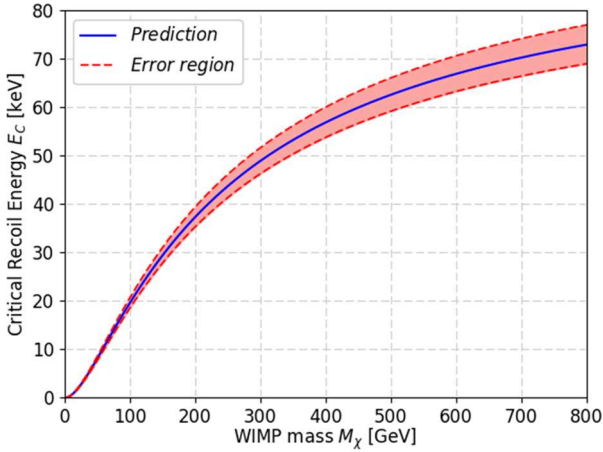

Figure 8 - Critical energy E_c as a function of WIMP mass M_χ for a xenon based detector. Calculated using a simplified SHM distribution for WIMP masses in the range of 0 to $800\,\text{GeV}$.
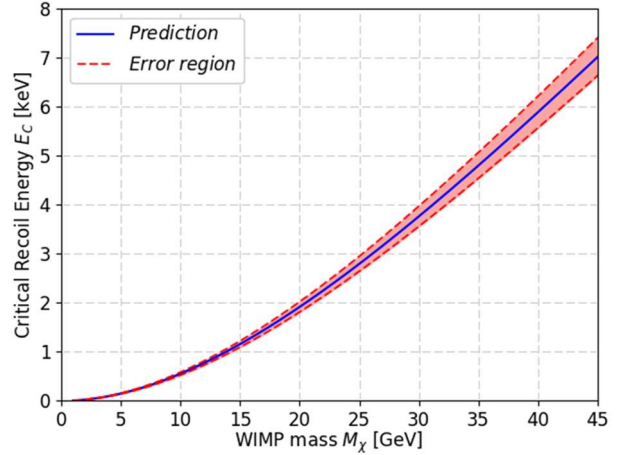
Figure 9 - Critical energy E_c as a function of mass M_χ for a xenon based detector. Calculated using a simplified SHM distribution for WIMP masses in the range of 0 to $45\,\text{GeV}$.

We can be see from figures 8 and 9 that the recoil energy for which the amplitude of detection modulation is zero is higher for larger WIMP masses. The exact form of these graphs is dependent on the detector particle being used.

Graphs such as these make it is possible to constrain the mass of the WIMP particles through direct detection experiments. If, for example, a direct detection experiment which detects nuclear recoils above some threshold energy E_{th} observes an annular peak in June then the critical energy must be lower than the threshold energy. This means that the WIMP mass must also be lower that the mass E_{th} relates to through the critical energy curve.

From figure 8 we see that the error in these constraints becomes significant for higher WIMP masses ($M_\chi \gtrsim 400\,\text{GeV}$). As the critical energy only depends on the mean inverse speed the only errors in this prediction, assuming the model is accurate, are due to uncertainty in the speed of the Earth and Sun. The uncertainty in the value for the speed at which the Sun travels through the galaxy is significantly larger than that of the speed of the Earth around the Sun. The latter is therefore assumed to be comparatively negligible. Naturally, the error in the critical energy curve can be therefore be reduced by improving the precision in the value for the Sun's orbital velocity.

This method of finding the critical energy function can easily be extended to other detector types. Two of the other most important detector types are germanium, used by the CoGeNT and CDMS teams, and sodium iodide used by the DAMA team [11, 15, 12]. The most interesting differences in these detectors are seen in the WIMP mass region below $100\,\text{GeV}$ as shown in figure 10.
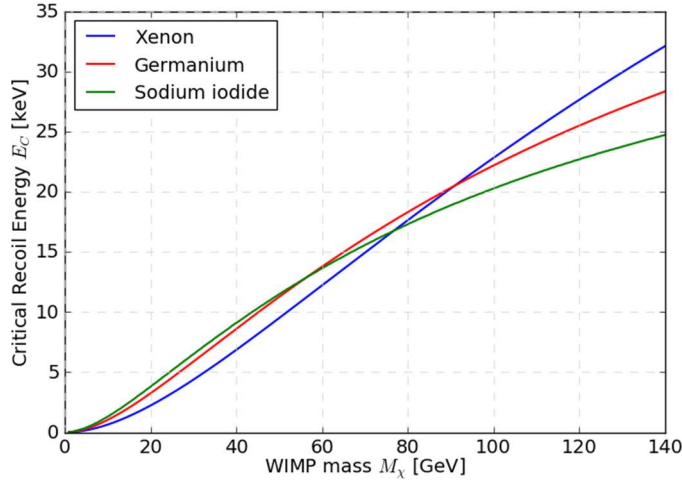
Figure 10 – Comparison of critical energy as a function of WIMP mass for a xenon, germanium and sodium iodide based detectors. Calculated using a simplified SHM distribution for WIMP masses in the range of 0 to 140 GeV

It can be seen that while the curves for each detector type are comparable they do have some distinct differences. This means that different detectors are better suited to measuring WIMPs of different masses. For example, if the mass of the WIMP particle is of a few tens of times larger than that of a proton then the critical energy will be highest for a germanium based detector.

B.   Improved SHM

The model considered so far can be made more physical by considering the implications of the escape velocity of dark matter. An analytical function can then be derived for the mean inverse speed (See section II.B.3)

1.   Differential Detection Rate

The differential detection rate can be calculated as a function of recoil energy as done for the simplified model (See section III.A.2). The results of the two different models are compared in figure 10, along with the relative error that arises as a result of neglecting the escape velocity of dark matter.
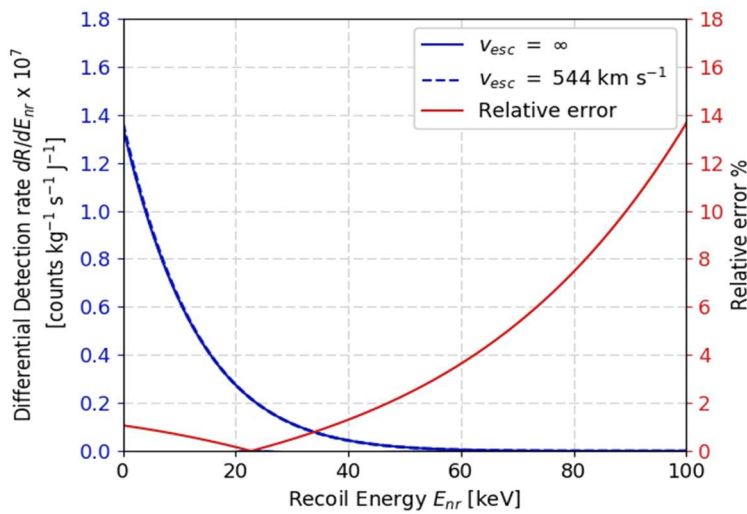

Figure 11 – Blue: Comparison of the predicted differential detection rate in June as a function of nuclear recoil for SHM distributions that omit and include the escape velocity of dark matter. Rate calculated energy for a WIMP mass of $70\,\mathrm{GeV}$ detected by a xenon based detector. Red: Relative error arising from not considering the escape velocity of dark matter.

12

It can be seen from figure 10 that the detection rate predicted by the two different models is very similar. The differences are highlighted by the relative error which becomes significant at high recoil energies. However, since the detection rate at these high energies is so low the absolute error on the predicted rate is still very small. The strong similarity between the two curves highlights the validity of the infinite escape speed approximation.

Using the differential detection rate calculated for June and December for the two distributions the predicted amplitudes of modulation can also be calculated and compared as shown in figure 11. Since the amplitude passes through zero, the relative error presents a sharp discontinuity at the critical energy. To avoid this, the absolute error was calculated instead.
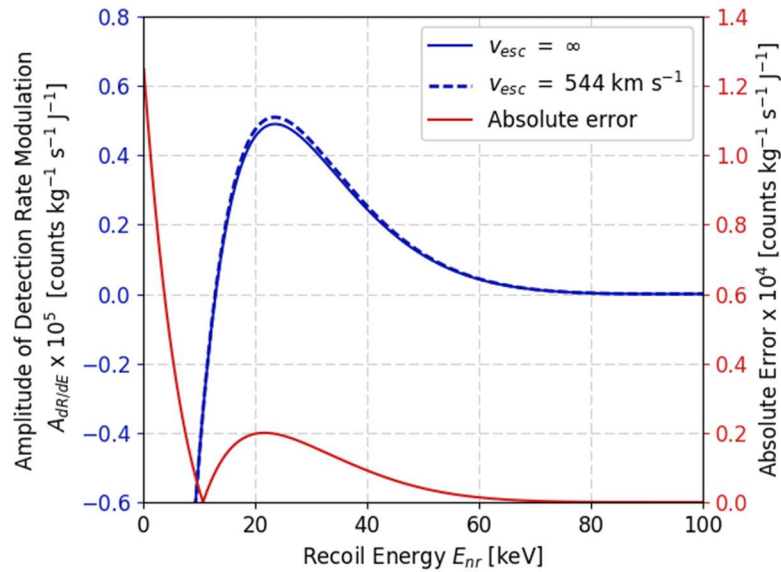

Figure 11 – Blue: Comparison of the predicted amplitude of detection rate modulation as a function of nuclear recoil for SHM distributions that omit and include the escape velocity of dark matter. Rate calculated energy for a WIMP mass of $70\ \text{GeV}$ detected by a xenon based detector. Red: Absolute error arising from not considering the escape velocity of dark matter.

The absolute error is found to be at its greatest for low recoil energies and tends towards zero as the recoil energy increases. Most importantly at the critical recoil energy of the original distribution there is a small non-zero error. This means that the critical energy function will be slightly different for the improved model.

2.   Critical Energy

We can then calculate the critical energy function for the new distribution. Calculating this using another root searching algorithm, the results from the two distributions can be compared as shown in figure 12.
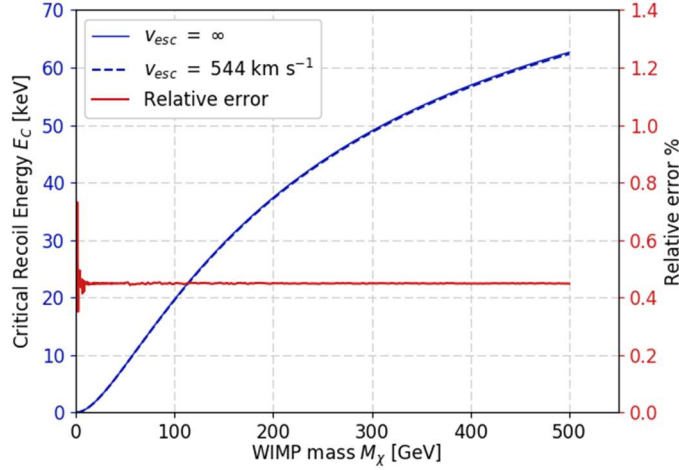

Figure 12 – Blue: Comparison of the predicted critical energy of a xenon bases detector as a function of WIMP mass for SHM distributions that omit and include the escape velocity of dark matter. Red: Absolute error arising from not considering the escape velocity of dark matter.

Similarly the detection rate and amplitudes shown in figures 10 and 11 respectively demonstrate that there is very little noticeable difference in the predicted critical energies using the two different distributions. Interestingly, aside from some 'anomalies' for WIMP masses close to zero, due to the nature of the root searching algorithm, the relative error arising from neglecting the escape velocity of dark matter remains constant 0.45% for all WIMP masses. This is because the escape velocity of the dark matter has the consistent effect of decreasing the critical energy by 0.45%. Again, this change is very small, highlighting the validity of the infinite-escape-velocity approximation. These predictions could be further improved by including considerations of the spin-dependent interactions in the calculation of the WIMP-nucleus scattering cross section.

C.   Dark Matter Stream

1.   Mean Inverse Speed

The distribution of a cold flow, such as a tidal stream, can be approximated to a Dirac delta function as given by equation 16. Using this approximation an analytical equation for the mean inverse speed can be found (See section II.B.3). The mean inverse speed of the simplified stream distribution is compared to that of the standard halo model in figure 13.
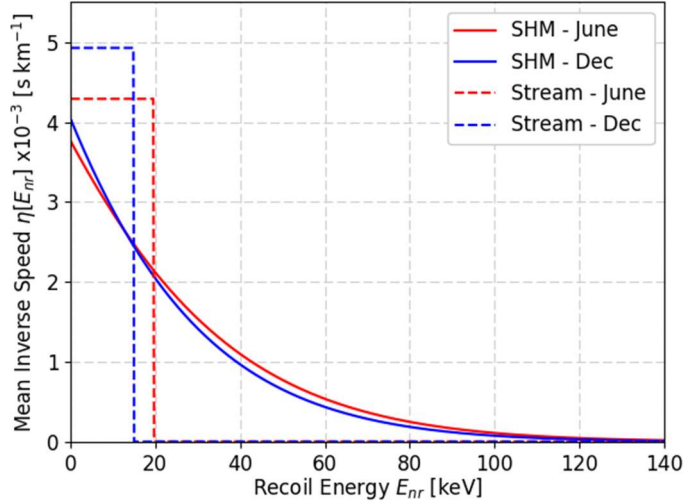
Figure 13 – Comparison of mean inverse speed for the Standard Halo Model and a cold flow stream of dark matter. Calculated for the case of a 70 GeV WIMP mass detected by a xenon based detector.

Naturally the sharp discontinuities shown in figure 13 for the cold flow are not very physical. The model could be improved by considering the cold flow as having some small, non-zero velocity dispersion instead of one which is negligible. This however, is beyond the remit of this investigation.

2.   Differential Detection Rate

The total differential detection rate is a linear sum of the contributions of the halo and the stream as shown in equation 18. For the purpose of demonstrating the potential impact of a stream on the annual modulation of dark matter detection an upper estimate of $0.2\rho_\chi$ is used for the density of dark matter within the flow. The resulting detection rate predicted for June and December is shown in figure 14.
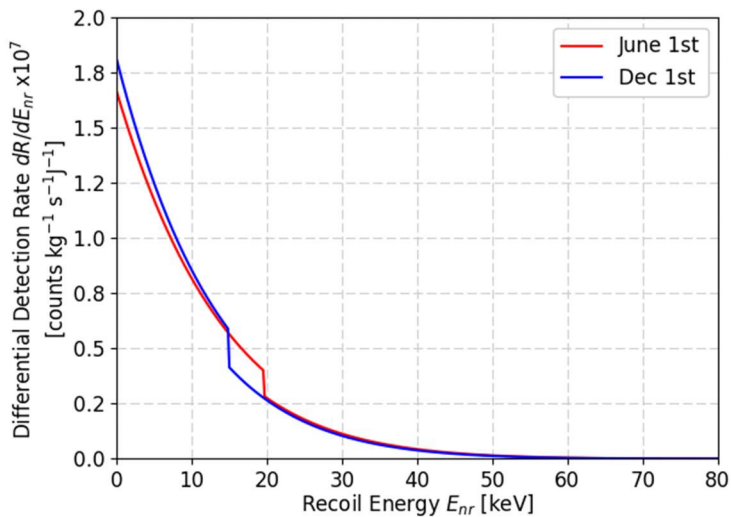

Figure 14 – Differential detection rate for the standard halo model with the addition of a cold flow stream of dark matter with a density 20% of that of the local halo. Calculated for the case of a 70 GeV WIMP mass detected by a xenon based detector.

From figure 14 it can be seen that the presence of a dark matter stream would have a significant impact of the difference between the detection rates in June and December. The stream would therefore have a significant impact on the annual modulation of dark matter detection. The amplitude of this modulation is compared with that of just the SHM in figure 15.
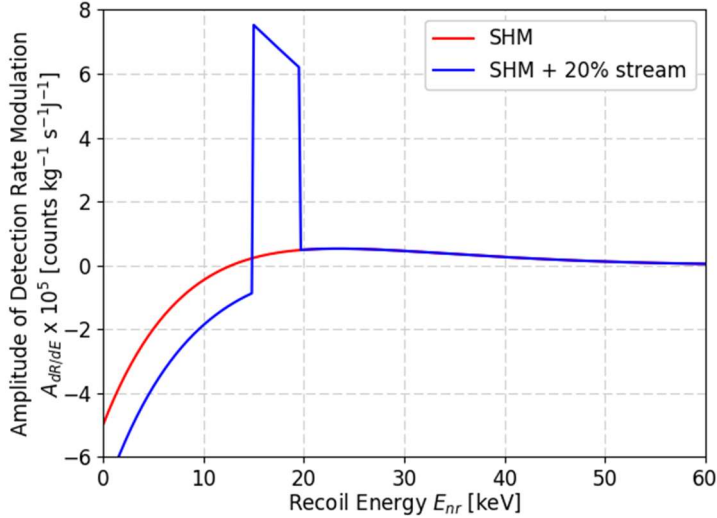
15

Figure 15 – Comparison of the amplitude of detection rate modulation for the SHM and the SHM with the addition of a cold flow stream of dark matter with a density 20% of that of the local halo. Calculated for the case of a 70 GeV WIMP mass detected by a xenon based detector.

Figure 15 shows that a stream would create a strong peak in the amplitude of modulation between two specific recoil energies. These energies relate to the detector speed $v_{\text{obs}}(t)$ in June and December through equation 1. Again, in reality these discontinuities would not be so sharp. The approximation for the distribution used is however sufficient for uncovering some of the primary impacts of a stream would have on the detection of dark matter.

The root of the combined distribution amplitude lies on the first of the two discontinuities. It can therefore be expected that such a stream would have a very significant impact on the critical energy curve. This influence would however be heavily dependent on the specific shape of the stream distribution. As such, the delta function approximation used here is not sufficient for investigating the potential impact a dark matter stream might have on the predicted critical energy curve. Such investigation is therefore beyond the remit of this report.

Figure 15 above does however highlight potential methods for determining the presence of a dark matter stream. In experiments in which the recoil energy of specific collision events can be measured, the stream could be inferred from the presence of a strong peak in the spectrum which deviates from the otherwise smooth curve described by the standard halo model. A less direct method comes from the total number of observed collision events. The presence of a stream would cause more dark matter particles to pass through the detector rather than / compared to the presence of the galactic halo alone. For the example case presented in figure 14, by integrating the differential detection rate with respect to the recoil energy, it is found that the total rate is on average 22% larger than predicted based on the SHM alone. For this specific case the increase in detection rate is a little higher than the fractional density increase of 20%. The converse is true for smaller WIMP masses. For example, for a WIMP mass of 30 GeV, all else equal, the total rate is 18% higher than SHM predictions. As such, without knowing the specific mass of the dark matter particles the density of a stream could not be estimated through detection rate alone.

IV.   Future of Direct Detection

The simplest way to improve the sensitivity of direct detection experiments is to increase the mass of the detector. This is exactly what was done by DEAP3600 and XENON1T who are expected to release their results later this year [26]. These detectors have maximum sensitivities of $\sigma_{SI} \sim 10^{-46} \, cm^2$ and $\sigma_{SI} \sim 10^{-47} \, cm^2$ respectively [27, 28]. The latter presents a twofold order of magnitude improvement in sensitivity compared to the previous experiments presented in figure 2. This increase in sensitivity is driven by the increase in detector mass; the XENON1T detector uses about 2 tonnes of liquid xenon in contrast to the 161 kg used in the XENON100 experiment [10].

There is however a limit to the sensitivity of direct detection experiments. This is because detectors will soon be sensitive to interactions involving neutrinos. As a result neutrinos from our Sun will be able to contribute both electronic and nuclear recoils [26]. This additional background will have to be accounted for. One potential method for distinguishing between WIMPs and neutrinos comes from the modulation of their signals.

Since the WIMPs originate from the galactic halo the detection rate is expected to peak in June (See section II.B). In contrast since the primary source of neutrinos is the Sun their detection rate should peak in early January when the Earth makes its closest approach to the Sun. In addition to this, the detection of atmospheric neutrinos has also been found to peak around January [29]. As such, the detection of a peak in June would still be strong evidence for the presence of dark matter in the form of WIMPs. This highlights the continued importance of the use of the modulation of dark matter detection rates. It has also been suggested that combining the detection data collected using different detector target nuclei could enable more of the neutrino background to be subtracted [30].

V.   Conclusion

By modelling the velocity distribution for dark matter as a simple Maxwellian distribution it has been found that the rate of detection varies annually with a modulation that is dependent on WIMP speed. As such, a detector specific critical energy exists, at which the modulation amplitude is zero. This critical energy is calculated for some of the most common detector types. The phase in modulation of the dark matter detection can be related to a maximum/minimum critical energy which, using predictions of the critical energy dependence on WIMP mass, can be related to a maximum/minimum WIMP mass. By constraining the WIMP mass, this would help to further constrain the WIMP-proton scattering cross section.

Furthermore, by modelling the distribution of a stream of dark matter as a Dirac delta function, the potential impacts of such a stream on the modulation of dark matter detection was investigated. It was found that such a stream could significantly change the critical recoil energy. Therefore, if such a stream existed in our local galactic region neglecting its impacts could result in incorrect mass constraints. Methods for determining the presence of a dark matter stream were also discussed. Most importantly, the presence of a stream would result a sharp peak in the detected velocity distribution. This peak would be roughly centred at a recoil energy relating to a WIMP speed given by the streams velocity relative to the detector.

References

[1] Oort, J. (1932). The force exerted by the stellar system in the direction perpendicular to the galactic plane and some related problems. *Bulletin of the Astronomical Institutes of the Netherlands*, 6, p.249.

[2] Zwicky, F. (1937). On the Masses of Nebulae and of Clusters of Nebulae. *The Astrophysical Journal*, 86, p.217.

[3] Rubin, V. and Ford, W. (1970). Rotation of the Andromeda Nebula from a Spectroscopic Survey of Emission Regions. *The Astrophysical Journal*, 159, p.379.

[4] Leonardi, R., et al. (2014). Planck2013 results. I. Overview of products and scientific results. *Astronomy & Astrophysics*, 571, p.A1.

[5] Taylor, A., Dye, S., Broadhurst, T., Benitez, N. and van Kampen, E. (1998). Gravitational Lens Magnification and the Mass of Abell 1689. *The Astrophysical Journal*, 501(2), p.539.

[6] Jungman, G., Kamionkowski, M. and Griest, K. (1996). Supersymmetric dark matter. *Physics Reports*, 267(5-6), p.195-373.

[7] Aad, G. (2014). Search for Dark Matter in Events with a Hadronically Decaying W or Z Boson and Missing Transverse Momentum in pp Collisions at $\sqrt{s} = 8$ TeV with the ATLAS Detector. *Physical Review Letters*, 112(4) p.041802

[8] Cherry, J., Frandsen, M. and Shoemaker, I. (2015). Direct Detection Phenomenology in Models Where the Products of Dark Matter Annihilation Interact with Nuclei. *Physical Review Letters*, 114(23)

[9] Goodman, M. and Witten, E. (1985). Detectability of certain dark-matter candidates. *Physical Review D*, 31(12), p.3059.

[10] Aprile, E., et al. (2012). The XENON100 dark matter experiment. *Astroparticle Physics*, 35(9), p.573.

[11] Aalseth, C., et al. (2013). CoGeNT: A search for low-mass dark matter using p-type point contact germanium detectors. *Physical Review D*, 88(1), p.012002.

[12] Cerulli, R. (2017). DAMA annual modulation and mirror Dark Matter. *The European Physical Journal C*, 77(2), p.83.

[13] Lewin, J. and Smith, P. (1996). Review of mathematics, numerical factors, and corrections for dark matter experiments based on elastic nuclear recoil. *Astroparticle Physics*, 6(1), pp.87-92.

[14] Catena, R. and Ullio, P. (2010). A novel determination of the local dark matter density. *Journal of Cosmology and Astroparticle Physics*, 2010(08), p.4.

[15] Schönrich, R., Binney, J. and Dehnen, W. (2010). Local kinematics and the local standard of rest. *Monthly Notices of the Royal Astronomical Society*, 403(4), p.1829.

[16] Bovy, J., et al. (2012). The Milky Way's circular velocity curve between 4 and 14 kpc from APOGEE data. *The Astrophysical Journal*, 759(2), p.131.

[17] Freese, K., Lisanti, M. and Savage, C. (2013). Colloquium: Annual modulation of dark matter. *Reviews of Modern Physics*, 85(4), pp.1561-1579.

[18] Smith, M., et al. (2007). The RAVE survey: constraining the local Galactic escape speed. *Monthly Notices of the Royal Astronomical Society*, 379(2), p.755.

[19] Dohm-Palmer, R., et al. (2001). Mapping the Galactic Halo. V. Sagittarius Dwarf Spheroidal Tidal Debris 60° from the Main Body. *The Astrophysical Journal*, 555(1), p.L37.

[20] Freese, K., Lisanti, M. and Savage, C. (2013). Colloquium: Annual modulation of dark matter. *Reviews of Modern Physics*, 85(4), pp.1565-1566.

[21] Aprile, E., et al. (2012). Dark Matter Results from 225 Live Days of XENON100 Data. *Physical Review Letters*, 109(18), p.181301.

[22]Helm, R. (1956). Inelastic and Elastic Scattering of 187-Mev Electrons from Selected Even-Even Nuclei. *Physical Review*, 104(5), p.1466.

[23]Vietze, L., et al. (2015). Nuclear structure aspects of spin-independent WIMP scattering off xenon. *Physical Review D*, 91(4), p.043520.

[24]Akerib, D., et al. (2016). Improved Limits on Scattering of Weakly Interacting Massive Particles from Reanalysis of 2013 LUX Data. *Physical Review Letters*, 116(16), p.161301.

[25]Ahmed, Z., et al. (2011). Results from a Low-Energy Analysis of the CDMS II Germanium Data. *Physical Review Letters*, 106(13), p.131302.

[26]Undagoitia, T. and Rauch, L. (2015). Dark matter direct-detection experiments. *Journal of Physics G: Nuclear and Particle Physics*, 43(1), p.013001.

[27]Kuźniak, M., et al. (2016). DEAP-3600 Dark Matter Search. *Nuclear and Particle Physics Proceedings*, 273-275, p.340.

[28]Aprile, E., et al. (2016). Physics reach of the XENON1T dark matter experiment. *Journal of Cosmology and Astroparticle Physics*, 2016(04), p.027.

[29]Desiati, P., et al. (2017). Seasonal variation of atmospheric neutrinos in IceCube. In: *33nd International Cosmic Ray Conference*. pp.13-16.

[30]Ruppin, F. (2014). Complementarity of dark matter detectors in light of the neutrino background. *Physical Review D*, 90(8), p.083510.